Carbon Dots Prepared from Waste Wood and Residual Adhesive and Their Use as Catalysts for Hydrogen Production

Ji Wu,[a] Liang Zhao,[a,]* and Guohui Song [b]

DOI: 10.15376/biores.19.2.2417-2435

** Corresponding author: liangzhao@njfu.edu.cn; zl_06@126.com*

GRAPHICAL ABSTRACT

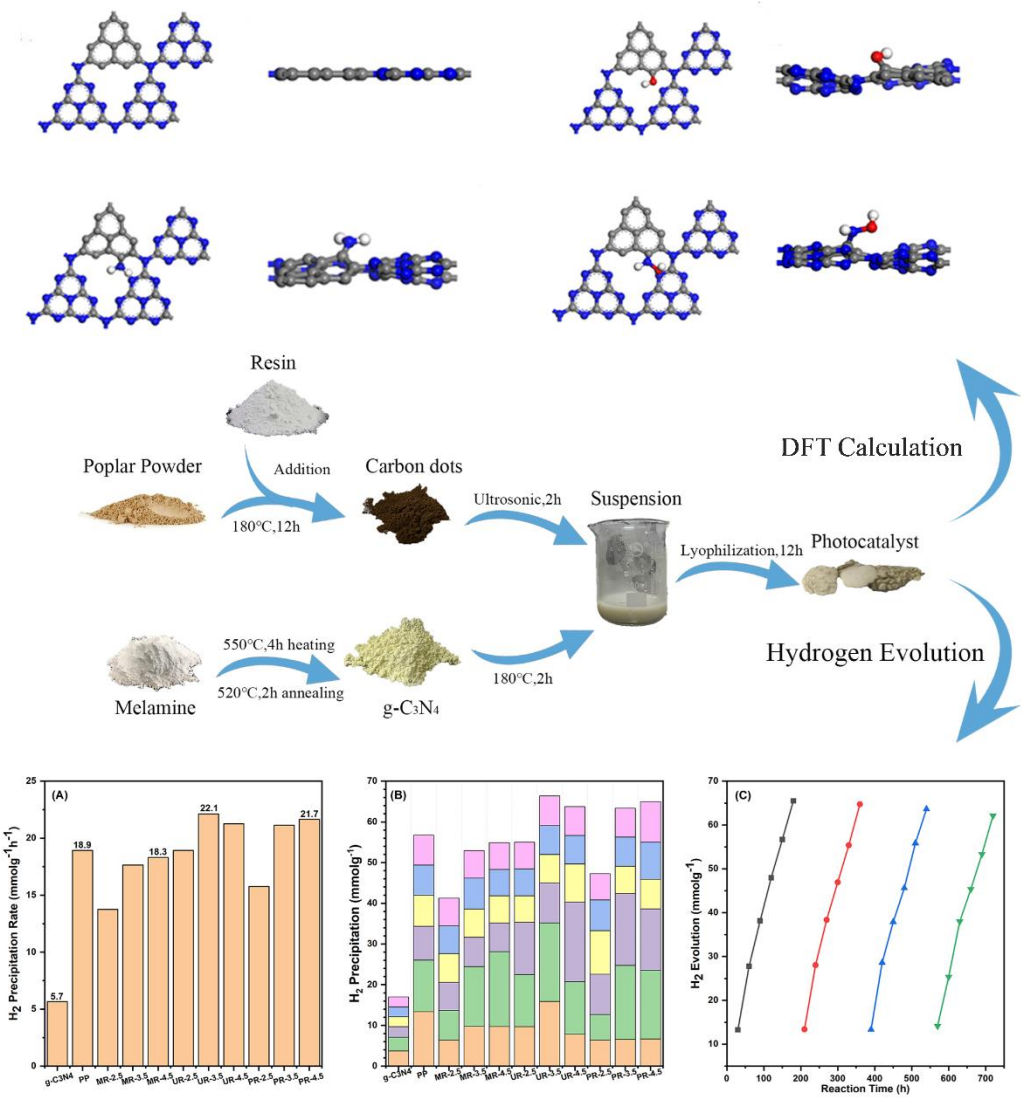

Carbon Dots Prepared from Waste Wood and Residual Adhesive and Their Use as Catalysts for Hydrogen Production

Ji Wu,[a] Liang Zhao,[a,*] and Guohui Song [b]

Large quantities of waste wood with residual resin adhesives are not recycled efficiently. To address this issue, waste wood with residual resin adhesives was synthesized into carbon dots (CDs) *via* a facile hydrothermal self-assembly method to enhance the H_2 evolution performance of graphite C_3N_4 (g-C_3N_4), a metal-free photocatalyst. Among all samples, the most significant enhanced sample was MCN-UF-3.5, which has an H_2 evolution of 22.1 mmol·g^{-1}·h^{-1}, which is 3.91 times that of unmodified g-C_3N_4. The band gap and recombination of photogenerated charges were both improved by the doping of CDs. Meanwhile, the DFT calculation showed that adding CDs, especially with the -NH_2 group, can significantly deform the structure and destroy the symmetry. This consequence implies an enhancement in the activity of the hydrogen evolution reaction, confirming the feasibility of the modification.

DOI: 10.15376/biores.19.2.2417-2436

Keywords: Waste wood; Residual adhesive; Carbon dots; g-C_3N_4; Photocatalytic; DFT

Contact information: a: Co-Innovation Center of Efficient Processing and Utilization of Forest Resources, College of Materials Science and Engineering, Nanjing Forestry University, Nanjing, 210037, China;
b: School of Energy and Power Engineering, Nanjing Institute of Technology, Nanjing, 211167, China;
** Corresponding author: liangzhao@njfu.edu.cn; zl_06@126.com*

INTRODUCTION

The proliferation of waste wood-based panels is a problem, but these materials could be used as valuable resources (Farjana *et al.* 2023). Due to the chemical pollutants and resin adhesives, the traditional disposal methods, such as landfilling and burning, are low-efficiency and high cost (Girods *et al*. 2008; Kim and Song 2014). These residual resins cannot be eliminated easily (Zhong *et al*. 2017). The residual resins hinder the modulus of rupture, modulus of elasticity, and internal bonding strength of remanufactured particleboards (Czarnecki *et al.* 2003). The residual resin and other compounds that are not conducive for recycling are difficult to handle efficiently and cost-effectively in the current common treatments. Therefore, there is an urgent need for a better way to utilize waste wood and its residual adhesive compounds.

Carbon dots (CDs) derived from biomass materials are emerging carbon nanomaterials with the advantages of advances in synthesis (Bian *et al.* 2016), hydrophilicity (Ehtesabi and Massah 2021), tunability (Ma *et al.* 2016), and optical properties (Liu *et al.* 2013), as well as a wide variety of raw materials, especially biomass (Li *et al.* 2020), whose sources are extensive and low-cost. CDs are commonly used in ion detection (Yang *et al.* 2022b), fluorescence imaging (Liu *et al.* 2017), photocatalysis (Sbacchi *et al.* 2023), and other applications. The main structure consists of a core

composed mainly of sp^2 hybridized regions, and a shell composed of sp^3 hybridized regions (Zhu *et al.* 2015). The shell composed of sp^3 endows CDs with the sites to bind functional groups such as -OH, -C=O, $-NH_2$, *etc*., which makes them well tunable (Xia *et al.* 2019). The sp^2-enriched nucleus of CDs is essential for photocatalytic reactions because of its large specific area and outstanding electron conductivity (Li *et al.* 2018).

Photocatalytic reactions include photocatalytic degradation and hydrogen evolution. The main principle of the photocatalytic hydrogen evolution reaction (Jafari *et al.* 2016) is the use of a catalyst to absorb photons to produce electron-hole pairs. Subsequently, H^+ formed at the catalytic site of the catalyst reacts with the electrons to produce hydrogen. Compared to metal catalysts, which are expensive and prone to secondary pollution, the two-dimensional material with rich sp^2 hybridization g-C_3N_4 is a more accessible and environmentally advantageous option. The g-C_3N_4 has the advantages of suitable band gap in visible light region, non-toxic feature, high chemical stability, and good elastic and tensile strength (Han *et al.* 2020), which means that it is suitable for photocatalytic hydrogen evolution (Zhao *et al.* 2015). However, the photocatalytic efficiency of the pristine g-C_3N_4 is unsatisfactory due to small specific surface area and easy complexation of photogenerated electrons (Mamba and Mishra 2016). At present, the main improvement directions for photocatalysts include (Fajrina and Tahir 2019) doping with heteroatoms, which can change the band gap structure, to enhance the absorption capacity in various wavenumber regions. Another option is to utilize the microstructure of nanoparticles with good mechanical properties and compatibility (Jia *et al.* 2023), such as SiC, as skeleton loading photocatalysts reduces the recombination of photogenerated electron-hole pairs (Wang *et al.* 2017).

Wood is made up of cellulose, semi-cellulose, and lignin. Cellulose was studied to be a good carbon source to prepare CDs (Souza *et al.* 2018). Lignin can offer O atoms and functional groups to enhance CDs performance. In addition, CDs prepared from waste wood can reduce preprocessing steps. So, the work in this study focused on providing a new route for the reuse of waste wood with residual adhesives. Carbon dots, which were prepared from waste wood, was used to modify g-C_3N_4 in order to enhance its photocatalytic H_2 evolution performance. Meanwhile, adding different kinds and ratio of adhesives to adjust photocatalysts performance, including phenolic (PF) resins, urea-formaldehyde (UF) resins, and melamine-formaldehyde (MF) resins. First principle calculation is used to emulate surface of photocatalysts to verify the mechanistic feasibility of the modification in this study.

EXPERIMENTAL

Materials

Melamine (≥ 99.6%, CP) was purchased by Lingfeng Chemical Reagent Co. Ltd. (Shanghai, China). Triethanolamine (TEOA, ≥ 99.0%, AR) was purchased by Sinopharm Chemical Reagent Co. Ltd. (Shanghai, China). Chloroplatinic acid hexahydrate (≥ 98.0%, AR) was purchased by Rhawn Reagent Co. Ltd. (Shanghai, China). Waste poplar was purchased by Maoyou Timber Co. Ltd. (Jiangsu, China). Urea-formaldehyde resin (UF), phenolic resin (PF) and melamine-formaldehyde resin (MF) were purchased by Zhongcheng Plastic Co. Ltd. (Zhejiang, China).

Synthesis Methods

The preparation method of CDs followed and was adapted from the hydrothermal method in previous studies (Wareing *et al.* 2021). The holistic synthesis process of CDs, g-C_3N_4 and photocatalyst is shown in Fig. 1(A). Specifically, 80 mesh poplar wood powder was mixed with different types of resins to form a mixture with a total weight of 2.5 g. The types of resins used in this study were urea-formaldehyde (UF), phenol-formaldehyde (PF), and melamine-formaldehyde (MF). The weight ratio of the resins in the mixture was 2.5%, 3.5%, and 4.5%, respectively. The mixture was dispersed in 50 mL deionized water. Then, after thorough stirring, the solution was transferred to a 100 mL Teflon-lined autoclave and heated at 180 °C for 8 h. Moreover, the suspension was centrifuged at 10000 rpm for 15 min to remove the bulk particles, leaving only the supernatant. Subsequently, the supernatant was dialyzed for 24 h using a dialysis bag with a molecular weight cut-off of 1000. Finally, the solution was lyophilized for 48 h and the obtained powder was collected and stored in a drying dish.

A total of 10 g of melamine was placed in a crucible of alumina and calcined in a tube furnace at 550 °C by 10 °C·min^{-1} heat rate for 4 h and annealed at 520 °C for 2 h. The samples were allowed to cool naturally to room temperature, and ground into 150-mesh powder.

For the preparation of photocatalysts obtained by functionalization of g-C_3N_4 coupled CDs, 100 mg of g-C_3N_4 was mixed with 10 mg of different kinds of CDs powder in 50 mL deionized water, which was then performed 2 h ultrasonic treatment and magnetically stirred for 2 h. Thereafter, the solution was transferred to a Teflon-lined autoclave and heated at 180 °C for 2 h. Following, the suspension was centrifuged at 10000 rpm for 2 min to obtain the lower precipitate after solid-liquid separation. Collected precipitate was lyophilized for 12 h. The final obtained powder is the photocatalyst denoted as MCN-x-y (modified g-C_3N_4). The x represents the kinds of resins added in preparation of CDs, and y represents the ratios of the CDs system. Samples without the CDs powder are named as g-C_3N_4, and ones with added unmixed CDs powder are named as MCN-PP (poplar powder-derived CDs).

Instruments

SEM (Reguluss8100, Hitachi), BET (BSD-PS(M), BEISHIDE), Raman spectrum (DXR532, Themor), FT-IR spectroscopy (VERTEX 80V, Bruker) and XPS (AXIS UltraDLD, Shimadzu) were used to obtain the morphology, microstructure, and surface elements chemical states of the samples. The optical and photoelectrochemical properties were characterized by a UV-vis diffuse reflectance spectra (Lambda 950, PE) and a photoluminescence (PL) emission spectra (FluoroMax-4, HORIBA). Hydrogen production was analyzed using a gas chromatograph (GC9790 Plus, Fuli).

Photocatalytic Hydrogen Evolution Experiment

For the photocatalytic H_2 evolution experiments, a 350 W cold xenon lamp with a light intensity set to 1100 W·m^{-2} was used as a light source to simulate solar irradiation. The reaction solution consisted of deionized water, 10 mL of TEOA, and H_2PtCl_6 at 3wt% to make up a total of 100 mL of the system. Next, 100 mg of catalyst was added to the solution, followed by purging with high-purity argon gas at a flow rate of 50 mL·min^{-1} and magnetic stirring for 60 min in a dark environment. After turning on the light source, the reaction gas products were collected using an aluminum foil gas bag, which was changed every 10 min. The gas products were passed into the GC for analysis.

DFT Calculation Details

The Cambridge Serial Total Energy Package (CASTEP) modules in BIOVIA Material Studios were used to emulate photocatalyst structures (Segall *et al.* 2002). All theoretical simulation calculations adopted Perdew-Burke-Ernzerhof (PBE) (Perdew *et al.* 1996a) functional within the generalized gradient approximation (GGA) (Perdew *et al.* 1996b). The ultra-soft pseudopotential and the norm-conserving pseudopotential were chosen to complete different parts of the calculations. The former has looser convergence conditions and was used for geometry optimization. The latter has stricter convergence and can obtain more accurate results. The properties of photocatalyst structures, such as band structure, the density of states (DOS), and potential, were calculated by the norm-conserving pseudopotential. Considering the Van der Waals interactions, the TS custom method was used for DFT+D to correct (Tkatchenko and Scheffler 2009). The cut-off energy was set with 400 eV for geometry optimization and 500 eV for properties (Yang *et al.* 2022a). Kohn-Sham wave functions were taken as a relativistic treatment. The parameters of convergence tolerance (Yang *et al.* 2022a): energy, max force, and max displacement were set as 1×10^{-5} eV·atom^{-1}, 3×10^{-2} eV·A^{-1}, and 1×10^{-3} A respectively, and SCF tolerance was set as 1×10^{-6} eV·atom^{-1}. In addition, given that hybrid functions have better performance in the band structure and DOS, HSE06 (Heyd *et al.* 2006), a hybrid function, was separately adopted in corresponding calculations.

RESULTS AND DISCUSSION

Morphology and Structure Characterization

SEM is commonly used to detect the microstructure and morphology of micrometer-sized catalysts. As displayed in Fig. 1(B), the major component of MCN-UF-3.5 photocatalyst was bulk g-C_3N_4, and the diameter was 15 to 20 μm.

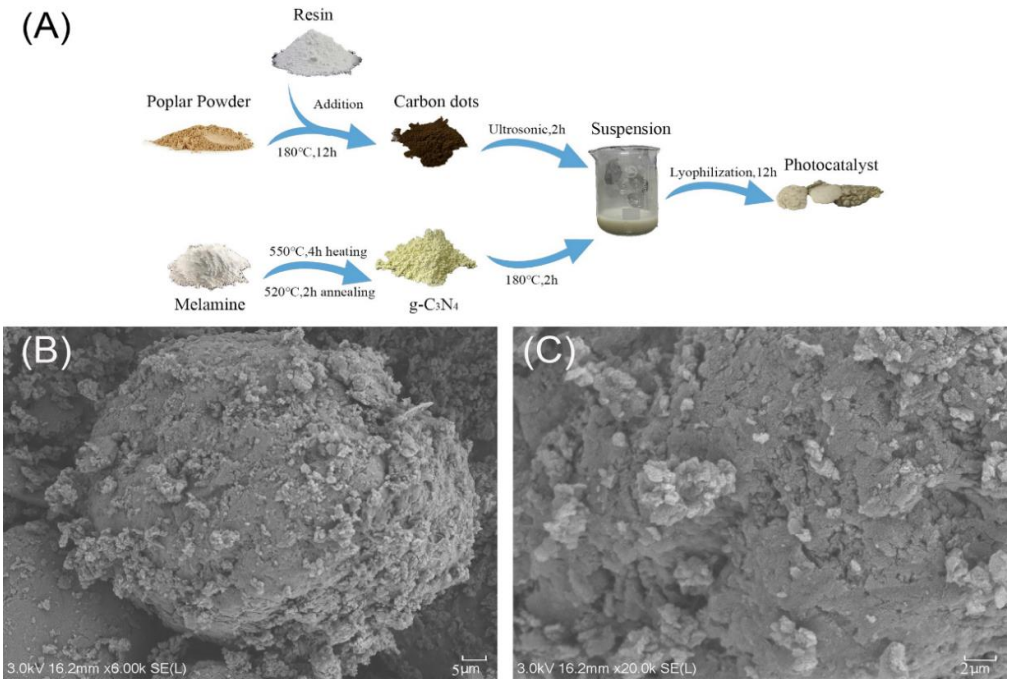

Fig. 1. (A) Synthesis of CDs, g-C_3N_4 and photocatalyst; (B, C) SEM images of MCN-UF-3.5

Numerous microparticle CDs were dispersed and attached to the surface of bulk g-C_3N_4. As shown in Fig. 1(C), the major component of the photocatalyst had lamellar features, composed of multiple ultrathin paper-fold sheets, which is the typical structure of g-C_3N_4. The morphology of the synthesized photocatalysts coincided with that reported by Cui *et al.* (2020). The morphology of CDs distributed on the surface was predominantly sphere-like or granular, matching the features in Singh's study (Singh *et al.* 2023). To better demonstrate the features of CDs, TEM, and other microscopy analysis will be carried out in the coming research. By measuring the particles in Fig. 1(C), it was known that their diameter was concentrated in the range of 1.4 to 0.2 μm or even smaller. These results suggested that the photocatalyst had the fundamental g-C_3N_4 structure, which could absorb radiation and emit electrons (Zhang *et al.* 2021), and the combination of CDs modified the surface.

The BET specific surface area of g-C_3N_4 and its modified samples were characterized by N_2 adsorption-desorption experiments. The isothermal curves are plotted in Fig. 2(A). As depicted in Fig. 2(A), both g-C_3N_4 and CDs doped samples exhibited type IV isothermal curves that did not reach the saturation plateau (Brunauer *et al.* 1938), indicating the presence of mesoporous architecture. The data revealed that MCN-UF-3.5, with the most significant specific surface area of 38.6 $m^2 \cdot g^{-1}$. The surface area of MCN-UF-3.5 was larger than that of g-C_3N_4 (10.3 $m^2 \cdot g^{-1}$) by 3.74 times. The previous studies reported that increased specific surface area is helpful to enhance photocatalytic performance (Alshammari *et al.* 2023). Therefore, the doping of CDs increased photocatalysts' specific surface area, making the 2-dimensional structure turn into the 3-dimensional structure (Zhu *et al.* 2017). This means that adding CDs improved the efficiency of charges transferring across the interface, positively affecting photocatalytic H_2 evolution.

Raman scattering is often used to obtain vibrational information specific to the chemical bonds in molecules. The Raman spectra in the work were excited at 780 nm using a dual laser system. Figure 2(B) shows Raman spectra of g-C_3N_4 and MCN-x-3.5 (x=PP, UF, MF, PF). MCN-UF-3.5 outperformed all other samples in terms of holistic intensity. The most substantial peak of samples in Fig. 2(B) was the peak located at 700 cm^{-1}. It is generally noted by the prior studies that this 700 cm^{-1} peak is a typical one caused by triazine ring vibrations with bent surface (Li *et al.* 2015). There was a weaker peak at 750 cm^{-1}, which was not universally presented in g-C_3N_4. Zinin *et al*. (2009) found that the 750 cm^{-1} peak mainly relates to the properties of raw materials used to synthesize. According to the report (Zinin *et al.* 2009), one typical peak of melamine, the raw material of the catalyst, was located around 750 cm^{-1}, which fits the regularity. Besides, the peak at 975 cm^{-1} had discrepancies with the simulation report results (Gonze *et al*., 2002) but was identical with Zinin's report (Zinin *et al.* 2009). As has been stated (Deifallah *et al.* 2008; Kroke *et al.* 2002), it was ascribed to the s-triazine breathing mode or polymorphs. As for the polymorphs, it was probably formed due to the destruction of the original structure of g-C_3N_4 by the ultrasonic treatment during synthesis. The peak with high intensity near 1340 cm^{-1} was a typical D band because of defects on the catalyst surface (Saraswat and Yadav 2020). These defects were caused by the surface modification by CDs, enhancing the sp^3 hybridization of the region. The cause of the peak formation at 1410 cm^{-1} was similar to the peak at 750 cm^{-1}. It was attributed to breathing and stretching of the ring (Meier *et al.* 1995). Furthermore, the undulating peak at 1590 cm^{-1} was the G band, mainly related to the sp^2 hybridization of C atoms (Grimm 2008). The prominent intensity of the peak at 1590 cm^{-1} of MCN-UF-3.5 clarified the higher electron conductivity than others (Luo *et*

al. 2019). It may be deduced from the phenomenon that MCN-UF-3.5 possessed a better capacity for H_2 evolution. The curve of g-C_3N_4 and MCN-PP had a more apparent G peak at 1410 cm^{-1} than other samples doped CDs. This phenomenon can be interpreted as related to ultrasonic treatment and doping of CDs. They did not destroy the structure of the triazine ring and s-triazine ring but accounted for the low intensity of the G peak.

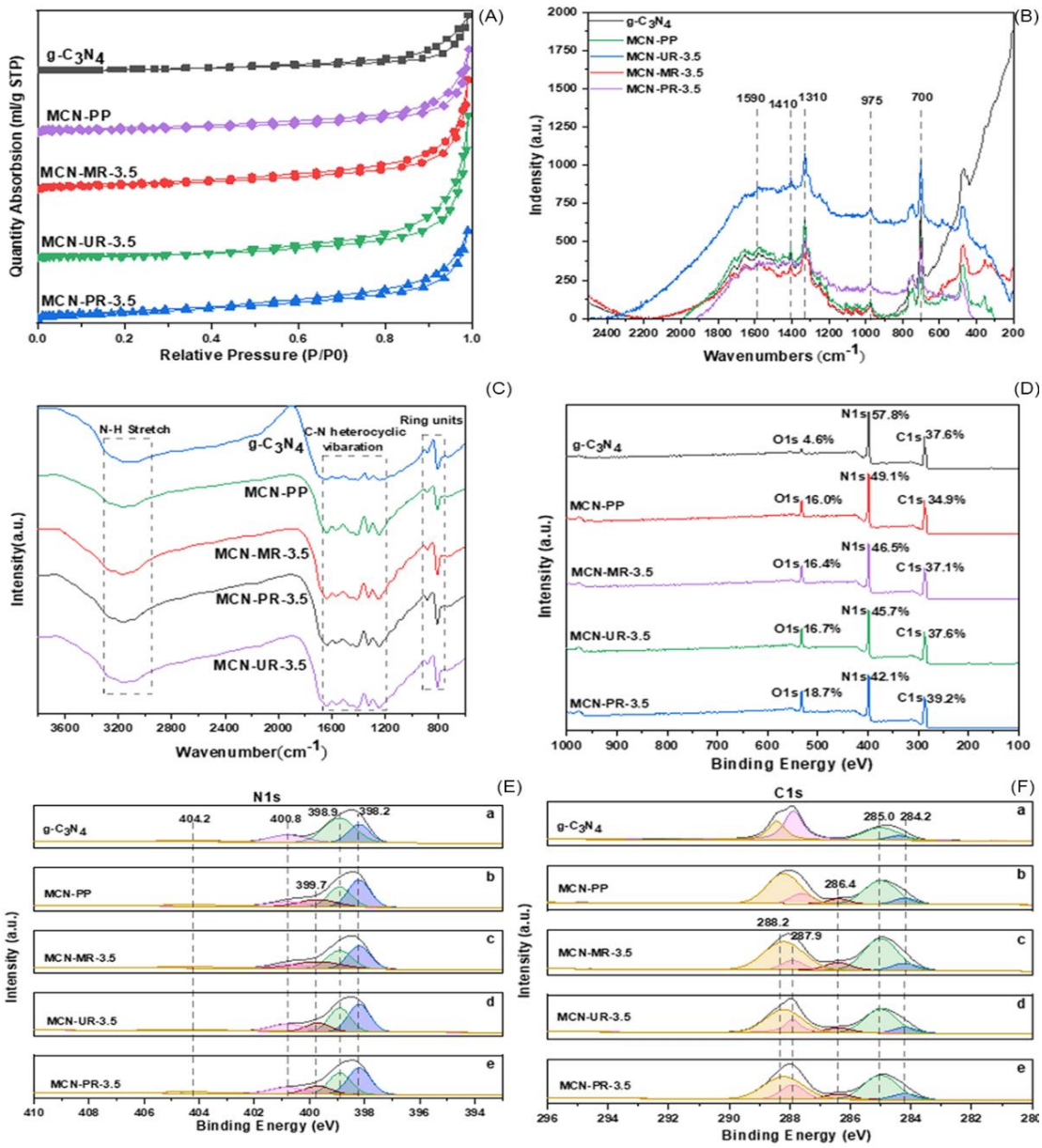

Fig. 2. (A) Nitrogen adsorption-desorption isotherms of samples; (B) Raman spectra (785 nm) of photocatalysts after background and offset corrections; (C) FT-IR spectra of g-C_3N_4 and different doped samples; (D) XPS survey spectra of samples; (E, F) High-resolution N1s and C1s spectra of photocatalysts

Analysis of information on molecule vibrations in FT-IR spectra referred to identifying the material molecules and functional groups on the surface. The FT-IR spectra of g-C_3N_4 and other samples doped with CDs are exhibited in Fig. 2(C). The key messages in Fig. 2(C) were concentrated in three sections, which were a section located in the range

of 3255 to 3050 cm^{-1}, a section ranging from 1650 to 1200 cm^{-1}, and a section within 900 to 800 cm^{-1} wavenumber range (Li *et al.* 2021). The first consisted of three scattered weak peaks: 3255, 3165, and 3082 cm^{-1}. Spectra in this area were analyzed to illustrate the information of the stretching vibrational characteristic of the substance. The peaks of three samples doped with diverse CDs had a higher intensity than the others. In particular, the peak at 3255 cm^{-1}, thought to be caused by the stretching of the O-H group (Cui *et al.* 2020; Li *et al.* 2021), was too weak to recognize in the pristine g-C_3N_4 but was notable in doped samples. Adding CDs synthesized by poplar powder and resins brought more O atoms into the photocatalyst, making the peak visible. The peak at 3165 cm^{-1} was regarded as the result of N-H stretching vibrations in uncondensed amino groups (Majdoub *et al.* 2020). There was an apparent disparity in peak intensity between MCN-UF-3.5 and the pristine g-C_3N_4. The stretching vibration of C-H bonds generally forms the peak located around 3040 cm^{-1} (Coates 2000). However, when the C atoms were located at the end of the molecular structure, C-H_2 bonds, whose stretching vibrational peak was found at 3085 cm^{-1} nearby (Ogita *et al.* 2004), would be formed. It can be inferred that C atoms at the edge positions in the structure destroyed by ultrasonic treatment reformed C-H_2 bonds during hydrothermal synthesis. The section, which was brought about by C-N heterocyclic vibrations ranging from 1650 to 1200 cm^{-1}, was subdivided into six peaks located at 1637, 1562, 1463, 1402, 1325, and 1236 cm^{-1}. The peak at 1637 cm^{-1} corresponded to the C=C bond of the aromatic ring skeleton, and the peak at 1469 cm^{-1} referred to the deformation of -CH_2 or the antisymmetric deformation of -CH_3 (Li *et al.* 2021). The last section, covering 900 to 800 cm^{-1} and composed of two peaks, represented the typical breath mode of triazine and s-triazine ring units, the skeleton of g-C_3N_4. The above analysis elaborated that the doping of CDs maintained the skeleton of g-C_3N_4. On this foundation, the treatment inducted more O atoms and reinforced the sp^3 hybridization of the surface.

The surface elemental chemical states of g-C_3N_4 and samples doped with CDs were detected using XPS. Figure 2(D) shows a survey scan spectra of five samples, which could be divided into three elemental solid components: O1s, N1s, and C1s. Among them, the intensity of O1s peak on g-C_3N_4 was weaker than others, and its peak area only occupied 4.6% of the total peak area of g-C_3N_4. The doping of CDs significantly increased the intensity of O1s, especially MCN-PF-3.5. The O1s peak area of MCN-PF-3.5 was up to 18.7% of the total peak area, owing to rich oxygenated functional groups on phenolic resin. The characteristics of the N1s spectra of four CDs doped samples were consistent. As presented in Fig. 2(E), five peaks located at 398.2, 398.9, 399.6, 400.8, and 404.2 eV were associated with sp^2 hybridization in C-N=C, pyridine N, N-$(C)_3$, N-H and charge effects triggered by stacking of π-bonds, respectively (Cheng *et al.* 2017; Fang *et al.* 2017). For the unmodified g-C_3N_4, the lower O content than the others blurred the boundary between the pyridine N peak and the N-$(C)_3$ peak, resulting in a distinct peak at 399.3 eV. This distinction meant that there was a weak modification of CDs adjusting the structure of g-C_3N_4, thus promoting photocatalytic performance. The C1s peaks of g-C_3N_4 and MCN-x-3.5 were divided into four and five sections, individually. The shared segments were located at binding energies of 284.2 and 285.0 eV, on behalf of the sp^2 hybridization part of carbon and the sp^3 hybridization part of C-C bonds (Chernyak *et al.* 2020). The trend demonstrated in Fig. 2(F) could be explained by the fact that these two peaks of CDs doped samples had higher intensity than the pristine g-C_3N_4. Oxygenated functional groups were attached to the surface broadened these peaks, increasing the difficulty of separating peaks. The peak located at 286.4 eV was not present in the unmodified g-C_3N_4 but in modified samples, indicating the C-O bonds (Li *et al.* 2021). There were two peaks at 287.9 and

288.2 eV. The former was related to the C=O bond, and the latter meant the sp^2 hybridization of N-C=N (Wang *et al.* 2018). There was a noticeable difference in the area of the peak located at 287.9 eV between samples of modified CDs with adhesives and others. O atoms generally were present in cured resins mixed with wood powder in the configuration of C-O-C, C-O-N, and O-H bonds. Although the solution was not in acidic conditions, the hydrothermal synthesis of waste wood with residual adhesives was reacted at higher temperatures and pressures than in the study of Liu *et al.* (2018). Due to the hydrolysis of cured resins, the original chemical bonds were broken, and C=O bonds were formed in such conditions. As described by Lukowsky (2002), ether bridges ($HNCH_2$-O-CH_2NH) in MF resins are more stable than methylene bridges ($NHCH_2$-NH). It was hard for O atoms to be restricted to the ether bridges to form C=O bonds. This concept was able to account for the lower peak intensity at 287.9 eV of MCN-MF-3.5 than samples modified by UF and PF. The peak unique to the unmodified g-C_3N_4 and MCN-PP had higher separation than others located at 287.6 eV, denoting the existence of the C=N combination. It could be concluded that the analysis of XPS spectra for each sample coincided with the results of FT-IR spectra. They both elaborated that the doping of CDs had modified the combination of chemical bonds on the surface without destroying the classical structure of the pristine g-C_3N_4, which enhanced the hydrogen evolution capacity.

Optical and Photoelectrochemical Properties

The photocatalyst, which occurred photon-excitation, caused the transition to excited states. Then, the emission of light or luminescence formed by the energy or photons released through the relaxation process is photoluminescence (PL). Thus the PL emission spectra were studied to understand the separation of photogenerated electron-hole pairs and recombination to study the optical properties of photocatalysts further. As shown in Fig. 3(A), the intensity of the unmodified g-C_3N_4 was much higher than that of others. The higher PL intensity of the photocatalyst represented more energy released through the recombination of electron-hole pairs than modified samples. This component energy was wasted and not transmitted to the photocatalyst surface for the hydrogen evolution reaction. The PL intensity of the unmodified g-C_3N_4 indicated the lower hydrogen evolution performance than others. Remarkable results relative to the problem of recombination of photogenerated electron-hole achieved by doping CDs could be deduced from Fig. 3(A). The data of time-resolved transient PL decay measured the lifetime of charge carriers. A shorter lifetime of charge carriers meant a faster rate of photogenerated electrons transferred to the photocatalyst surface.

Equation 1 calculates the final average lifetime of PL (Zhang *et al.* 2022),

$$\tau_{ave} = \frac{B_1\tau_1^2 + B_2\tau_2^2}{B_1\tau_1 + B_2\tau_2} \quad (1)$$

where τ_1 and τ_2 are the first-order fitting and the second-order fitting lifetime, and B_1 and B_2 correspond respectively to their normalized amplitudes (Chauhan *et al.* 2016). As shown by data listed in Table 1, modified samples obtained a shorter average PL lifetime than the unmodified g-C_3N_4, especially MCN-PF-3.5. Comparing MCN-PF-3.5 with the unmodified g-C_3N_4, the reduction of the PL lifetime was up to 31.2%. This result manifested that the time for the recombination of charge carriers became much less, and due to the increase in the utilization of photogenerated electrons, the number of unrecombined electron-hole pairs increased.

Table 1. Average Lifetime of Samples after Second-Order Fitting

Sample	g-C_3N_4	MCN-PP	MCN-MF-3.5	MCN-UF-3.5	MCN-PF-3.5
Lifetime (ns)	4.207	3.907	3.383	3.418	2.895

As a standard method to analyze the optical properties, UV-Vis DRS was detected to further investigate the electronic transition between energy levels g-C_3N_4 and samples doped with CDs. On the basis of the intensity that emerged in Fig. 3(B), it can be inferred that the doping of CDs obviously raised the absorbance of related samples in the vicinity of 275 nm and the visible light region. A recognizable peak appeared at 375 nm of all samples, adding CDs with residual resins. The peak was located in the near-ultraviolet region, symbolizing the transition of n-π*, which was contributed by chromophores, *e.g.*, C=O, C=N (Fang *et al.* 2017; Selmi *et al.* 2023). The feature of UV-vis DRS spectra of samples containing adhesives conformed to that of C1s spectra. In addition, the presence of chromophores made red shift occur on the highest characteristic peak due to the promotion of the conjugation effect. Consistent with Shibayama *et al.* (2019), the better absorbance performance of the photocatalyst in the visible light region can drive photocatalytic evolution better because of the more efficient utilization of irradiation. The curves of Tauc plots (Davis and Mott 1970), whose data was solved by Eq. 2 (Chen *et al.* 2016) for the g-C_3N_4 direct transition photocatalysts, are plotted in Fig. 3(C),

$$E_g = h\nu - \frac{(\alpha h\nu)^2}{A^2} \quad (2)$$

where Eg is band gap energy, h is Planck's constant, ν represents light frequency, and A means a constant. As seen in Fig. 3(C), the band gap energy of several samples were 2.79, 2.74, 2.73, 2.65, and 2.78 eV, corresponding to the unmodified g-C_3N_4, MCN-PP, MCN-MF-3.5, MCN-UF-3.5, and MCN-PF-3.5, respectively. It was easier for the photocatalyst with a narrower band gap to absorb the charge with lower energy and react. Based on the results, the doping of CDs, particularly with UF resins, significantly narrowed the band gap and made photocatalytic evolution react more efficiently.

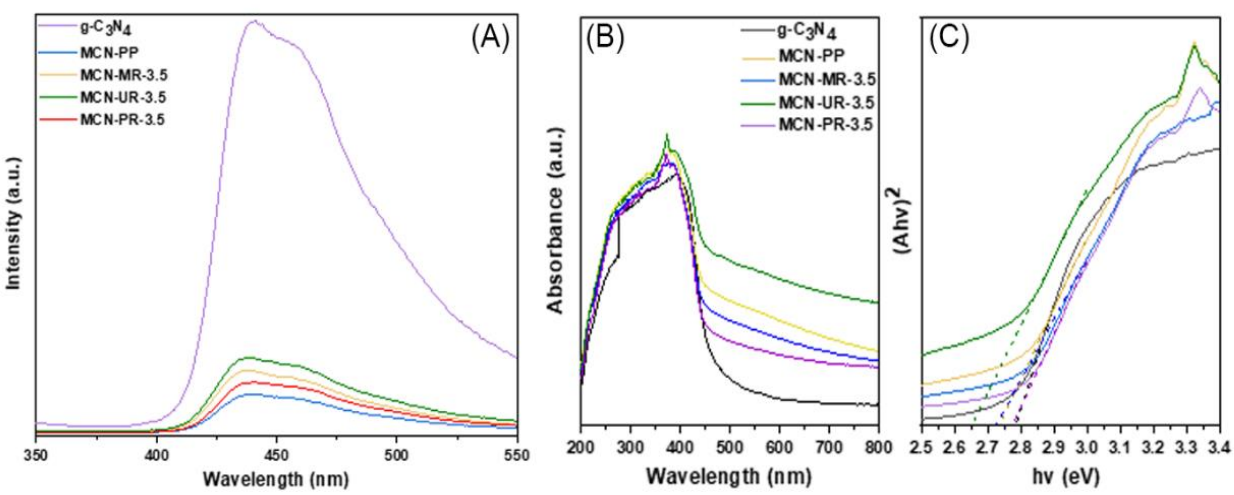

Fig. 3. (A) PL spectra with an excitation (ex) wavelength of 300 nm; (B) UV-Vis DRS spectra; (C) Tauc-plots and bandgap information of g-C_3N_4 and MCN-x-3.5 (x=PP, MF, UF, PF)

Photocatalytic H_2 Evolution

All experiments, including photocatalytic H_2 evolution and stability, were conducted under visible light irradiation (≥420 nm). Before the start of irradiation, 3 wt% Pt was added into the system for attaching the surface of photocatalysts and providing sites for the adsorption of H^+ and H_2. Moreover, 10 mL of TEOA was added to the reaction system as a sacrificial agent. As shown in Fig. 4(A, B), the doping of CDs conspicuously promoted the H_2 evolution of photocatalysts. The average H_2 evolution rate of the unmodified g-C_3N_4 was 5.7 mmol·g^{-1}·h^{-1}, and that of MCN-UF-3.5 was 3.91 times as large as the former's (22.1 mmol·g^{-1}·h^{-1}). Despite the samples being doped with CDs, there were some differences between them. The H_2 evolution of the MCN-UF-3.5, the optimum performance photocatalyst, was 17.0% better than that of MCN-PP. It can be concluded that adding CDs containing UF to photocatalysts was more capable of promoting H_2 evolution than CDs without resins. The samples containing MF were similar to those containing PF, following the same trend: as the amount of doping increased, the hydrogen yield also increased. However, MCN-PF-y had more tremendous advantages than MCN-MF-y. MCN-PF-4.5 had a rate of 21.7 mmol·g^{-1}·h^{-1}, which was 18.3% higher than MCN-MF-4.5. The structure of MF resin resembled that of melamine, which was used to synthesize g-C_3N_4. That is why adding MF resin was challenging to generate a variation in the unmodified photocatalyst. Fewer structural changes eventually led to the lower H_2 evolution. In the case of PF resins, the augmentation of H_2 evolution brought in by increased usage retarded when the blended amount was up to 4.5%. Because of the insolubility of PF resin, as pointed out by Shibayama *et al*. (2019), excess usage may hinder the adsorption of water molecules by photocatalysts. Also, the H_2 evolution of MCN-UF-4.5 was reduced by 4.1% compared to MCN-UF-3.5, elucidating that the superfluous addition of UF degraded the H_2 evolution as well. According to Liu *et al.* (2018), excessive addition of UF may increase in alkaline concentration to hinder the further decomposition during the hydrolysis process.

Based on the H_2 evolution performance, MCN-UF-3.5 was selected as the object for the photocatalytic stability experiment. Four cyclic reactions lasting three hours with identical reaction conditions, as described in Section 2.2, constituted the photocatalyst stability experiment with a total duration of 12 h. Before each loop began, 10 mL TEOA was extra replenished into the reaction system. As shown in Fig. 4(C), the evolution of each cycle was close and demonstrated a slight downward trend from a holistic view. The H_2 evolution of the initial and final cycles were 65.5 and 62.1 mmol·g^{-1}, separately. The reduction between the initial and the final was 5.2%, suggesting the high stability of MCN-UF-3.5 against photocorrosion.

Combined analysis of characterization and experimental results, it was reasonable to expect that the residual resin adhesives and groups isolated from them had modified the photocatalyst surface. To sum up, the modification of CDs with adhesives to photocatalysts covered three aspects. Firstly, corresponding to the Raman spectra, the higher degree of sp^2 hybridization in samples that had CDs added with adhesives enhanced the electron conductivity. So, the activity of the hydrogen evolution reaction got higher. Secondly, the optical properties detected by PL and UV-Vis DRS spectra were embellished by adding CDs. The better absorption of visible radiation and the narrower band gap can generate more electrons for the H_2 evolution reaction. Finally, as displayed in Table 1, the shorter lifetime restrained the possibility of the electron-hole pairs' recombination, lifting the utilization of photogenerated electrons. Due to these modifications, the amounts of H_2

evolution of samples doped with CDs were improved and distinguished from the pristine g-C_3N_4 and even MCN-PP.

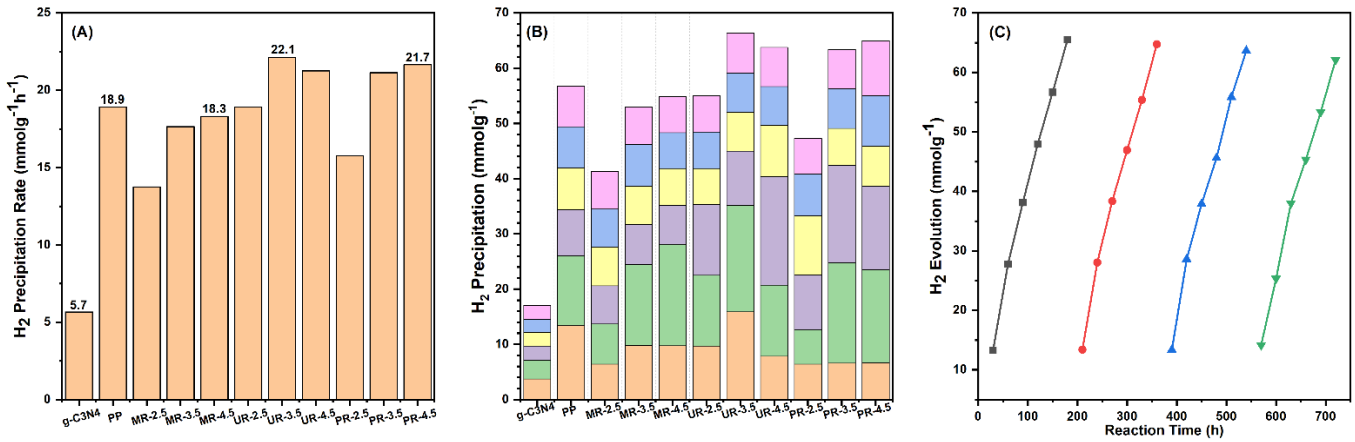

Fig. 4. (A) Photocatalytic H_2 evolution of different samples; (B) Photocatalytic H_2 evolution rate; (C) Stability experiment of H_2 evolution on MCN-UF-3.5 under visible light (⩾420 nm)

DFT Calculation and Discussion on Photocatalytic Mechanism

The evidence from the characterization and experimental work confirmed the effective modification of photocatalysts by CDs. However, there were still distinctions between photocatalysts doped with CDs mixed with different residual resins. For the purpose of investigating the influences of the addition of CDs, DFT was taken as the tool. Before modeling the photocatalyst modified by CDs, the band structure, partial density of states (PDOS), and electrostatic potential were calculated to certify the coincidence of the realistic structure and the build. As plotted in Fig. 5(A), the band gap of g-C_3N_4 was 2.79 eV, coinciding with that of the Tauc-plot curve in Fig. 3(C). The electrostatic potential determined the inclination of the photocatalyst to be excited. The potential of the pristine g-C_3N_4 model displayed in Fig. 5(B) was 5.83 eV, which was too high to be excited due to the absence of surface defects. Figures 5(C) and 5(D) demonstrated the PDOS spectra of C and N atoms. Linking and analyzing Fig. 5(A) and Fig. 5(C, D), for the unmodified g-C_3N_4, the valence band maximum was mainly dominated by N-2p orbitals. The conduction band maximum was mainly occupied by C-2p and N-2p orbitals. Compared with the Fermi level in Fig. 5(B), the valence band of the unmodified g-C_3N_4 was far from the Fermi level, implying the lower mobile carrier density and poor charge transfer ability. This result agreed with the data of the PL lifetime. Regarding Mulliken charges, all C atoms in g-C_3N_4 carried a positive charge of 0.54 eV. Most N atoms had a negative charge of 0.41 eV, and the joint N had a negative charge of 0.32 eV. The electronegativity center was deduced to sit in the region enclosed by triazine rings.

The structures of samples doped with CDs were built on the unmodified g-C_3N_4. The internal portion of CDs was composed of sp^2 hybridization C, and the external was constructed by sp^3 hybridization C, which can connect with functional groups. As shown in Fig. 5(C, D), CDs replaced one triazine ring to adjust the surface. The surface structure was nearly unchanged because of the resemblance of the partial double bonds of triazine rings and CDs. Studies by Norskov *et al*. (2004) and Yang *et al*. (2022) pointed out that the process of optical H_2 evolution reaction can be detached into four one-electron steps. Based on the reaction steps, *OH is the crucial step in the optical H_2 evolution reaction, which exists in both transformation paths. So, the -OH group was selected to adhere to the

edge of CDs to stimulate the absorption of the -OH group on the surface. Furthermore, for the sake of figuring out the superiority of the doping of the UF, the $-NH_2$ group, the typical functional group of UF, was attached to the CDs to compare with the resin-free model. The top and front views of all structures are displayed in Fig. 5(E-L). For ease of exposition and understanding, the C atom on the leftmost side of CD connected to the N atom in the s-triazine ring formed an internal angle labeled as $\angle_{LC-C-C}$. In the same way, the right one was marked as $\angle_{RC-C-C}$.

The resin-free photocatalyst, as shown in Fig. 5(E), was the most stable structure, whose surface was as flat as the pristine g-C_3N_4. The C-N bond length of CD connecting with s-triazine rings was 1.40 Å, close to that of the s-triazine rings' interconnection. Moreover, CDs structure possessed symmetry, and $\angle_{LC-C-C}$ was 110.31°. These results showed a tight combination between CD and s-triazine rings, and the structure of CD was stretched somewhat in their respective directions by multiple s-triazine rings. The original leveled structure was destroyed when the -OH group was adsorbed on CDs, as shown in Fig. 5(G). The geometric structure of free water molecules in the liquid phase can be described, as the bond length of O-H was 0.96 Å, and the angle of H-O-H was 109.50°. Compared to free water molecules, 0.98 Å in Fig. 5(G) was longer, and 108.95° was narrower. It could be inferred that *OH had a higher activity than free water molecules. Also, the structure of the CD section became asymmetrical. $\angle_{LC-C-C}$ in Fig. 5(I) was 102.80°, and $\angle_{RC-C-C}$ was 115.69°, which was more similar to the original. The bond on the left and right was 1.42 Å and 1.45 Å, respectively. The movement of bonds and angles proved that the right structure was more stable but not as tightly bound to the s-triazine ring as the left. Moreover, the binding energy of C-O was -0.70 eV.

For the CDs with the $-NH_2$ group, as depicted in Fig. 5(I), there was a radical deformation from the top view compared to the structure in Fig. 5(E). The degree of $\angle_{LC-C-C}$ and $\angle_{RC-C-C}$ was 97.59° and 123.88°, respectively, illustrating that the deformation got greater than that of the structure in Fig. 5(E), and the activity rose. The length of the C-N bond between CD and the $-NH_2$ group was 1.35 Å, which was consistent with that in s-triazine rings. When the -OH group was adsorbed on $-NH_2$ of CD, $\angle_{LC-C-C}$ was 103.70°. The length of the bond linking CDs and H-N-OH was 1.37 Å, and the length of O-H was 0.99 Å. These bonds were more extended than that without the adsorption of the -OH group. The binding energy of the O atom reduces to -0.39 eV, explaining that it was easier for CDs with the $-NH_2$ group than CDs to react. As mentioned in the study of Yin *et al*. (2018), it was neither too tightly adsorbed for such binding energy, making it challenging to desorb, nor too low in binding energy, making adsorption difficult. The site on $-NH_2$ was suitable for extracting -OH from water molecules and dismantling H^+ and electrons for the subsequent reaction.

All structures obtained by calculations revealed that $-NH_2$ groups on CDs can pull CDs out from the plane and deform the surface. Regarding mechanistic feasibility, the above essential calculation results explained that adding CDs with UF resin altered the surface structure and made it more active for adsorption and reaction.

Besides, though methylene bridges are unstable, more NH_2 groups can be produced by the rupture of methylene bridges. In all samples modified by CDs with adhesives, the H_2 evolution performance of MF was the worst. The primary cause of this appearance was ascribed to the units of MF intended for paper impregnation. To maintain suitable viscosity

and penetration, the prepolymers of MF, made up of three to five oligomers of melamine units, possessed low molecule weight (Henriques *et al.* 2017). Therefore, many MF prepolymer patterns were typically formed by chain and isotropic growth (Al-Moameri *et al.* 2021). For the situation caused by chain growth, many H-N-OH or -NH_2 groups were exposed to the outside of the structure, contributing to improving the H_2 evolution. However, when the prepolymers were formed by isotropic growth, more free functional groups were formed ether bridges by the literation of water molecules. These ether bridges were stable and were not sp^2 hybridized, which means that they cannot enhance the reaction activity in the same way as the structure of PF.

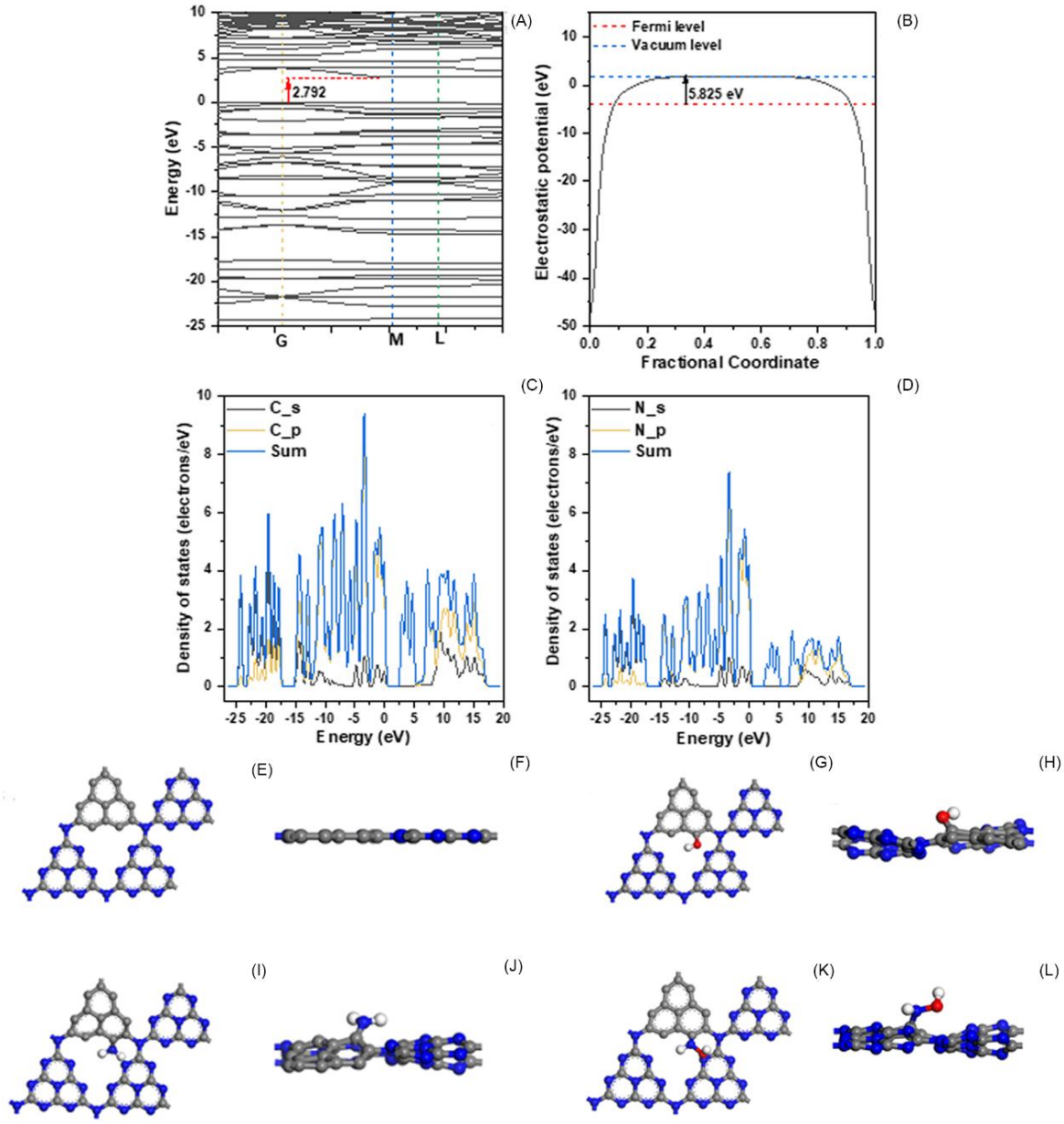

Fig. 5. (A) Band Structure and bandgap; (B) Electrostatic potential of g-C_3N_4 optimized; (C, D) Calculated density of states of different elements in g-C_3N_4; (E-L) Top and across view of optimized geometries of g-C_3N_4 doped CDs with different groups, including (E, F) resin-free CDs; (G, H) CDs with -OH; (I, J) CDs with -NH_2; (K, L) CDs with H-N-OH (Color scheme: C, grey; N, blue; O, red; H, white)

CONCLUSIONS

1. In this research, g-C_3N_4 modified by CDs exhibited superiority over the unmodified in photocatalysis-related indicators, for example, band gap and PL lifetime. Under visible light irradiation, the average evolution of pristine g-C_3N_4, MCN-PP, MCN-MF-4.5, MCN-UF-3.5, and MCN-PF-4.5 were 5.7, 18.9, 18.3, 22.1, and 21.7 $mmol \cdot g^{-1} \cdot h^{-1}$, respectively. MCN-UF-3.5, the best-optimized sample, was up to 391% higher than the unmodified g-C_3N_4 and 117% higher than MCN-PP. Such results elucidated the finding that the environmentally friendly CDs prepared from waste wood had a positive enhancement effect on the unmodified g-C_3N_4. Also, the addition of UF and PF resin in moderation became a factor to further promote the efficiency of photocatalytic H_2 evolution performance.
2. This research put forward a convenient hydrothermal self-assembly method to drive waste wood with residual resin adhesives into CDs to enhance the performance of g-C_3N_4.
3. The surface morphology of photocatalysts obtained by DFT calculations certified that doping groups on resin could adjust surface patterns and increase the activity of photocatalysts, corresponding to the experimental results.
4. In summary, this study provided a new reusage opportunity and method for utilizing waste wood with residual resin adhesives to design and synthesize green, efficient metal-free photocatalysts with g-C_3N_4, which can be extended in many applications such as solar energy reserves, photovoltaic equipment, and water pollution treatment.

ACKNOWLEDGMENTS

This study was supported by the Key Research and Development Program of Jiangsu Province (BE2023361). The authors acknowledge the support of the Advanced Analysis and Testing Center of Nanjing Forestry University.

REFERENCES CITED

Al-Moameri, H., Jaf, L., and Suppes, G. J. (2021). "Simulation approaches for the mechanisms of thermoset polymerization reactions," *Molecular Catalysis* 504, article 111485. DOI: 10.1016/j.mcat.2021.111485

Alshammari, K., Alotaibi, T., Alshammari, M., Alhassan, S., Alshammari, A. H., and Taha, T. A. M. (2023). "Synthesis of sulfur@g-C_3N_4 and CuS@g-C_3N_4 catalysts for hydrogen production from sodium borohydride," *Materials* 16(12), article 4218. DOI: 10.3390/ma16124218

Bian, Y., He, B., and Li, J. (2016). "A one-step hydrothermal method of nitrogen-doped graphene quantum dots decorated graphene for fabrication of paper-based fluorescent composite," *Bioresources* 11(3), 6299-6308. DOI: 10.15376/biores.11.3.6299-6308

Brunauer, S., Emmett, P. H., and Teller, E. (1938). "Adsorption of gases in multimolecular layers," *Journal of the American chemical society* 60(2), 309-319.

Chauhan, H., Kumar, Y., Dana, J., Satpati, B., Ghosh, H. N., and Deka, S. (2016). "Photoinduced ultrafast charge separation in colloidal 2-dimensional CdSe/CdS-Au

hybrid nanoplatelets and corresponding application in photocatalysis," *Nanoscale* 8(34), 15802-15812. DOI: 10.1039/c6nr03610d

Chen, X., Wei, J., Hou, R., Liang, Y., Xie, Z., Zhu, Y., Zhang, X., and Wang, H. (2016). "Growth of g-C_3N_4 on mesoporous TiO_2 spheres with high photocatalytic activity under visible light irradiation," *Applied Catalysis B: Environmental* 188, 342-350. DOI: 10.1016/j.apcatb.2016.02.012

Cheng, R. L., Jin, X. X., Fan, X. Q., Wang, M., Tian, J. J., Zhang, L. X., and Shi, J. L. (2017). "Incorporation of N-doped reduced graphene oxide into pyridine-copolymerized g-C_3N_4 for greatly enhanced H_2 photocatalytic evolution," *Acta Physico-Chimica Sinica* 33(7), 1436-1445. DOI: 10.3866/PKU.WHXB201704076

Chernyak, S., Podgornova, A., Dorofeev, S., Maksimov, S., Maslakov, K., Savilov, S., and Lunin, V. (2020). "Synthesis and modification of pristine and nitrogen-doped carbon dots by combining template pyrolysis and oxidation," *Applied Surface Science* 507, article 145027. DOI: 10.1016/j.apsusc.2019.145027

Coates, J. (2000). *Interpretation of Infrared Spectra, A Practical Approach*, Wiley.

Cui, S. C., Li, R., Pei, J. Z., Wen, Y., Li, Y., and Xing, X. Y. (2020). "Automobile exhaust purification over g-C_3N_4 catalyst material," *Materials Chemistry and Physics* 247, article 122867. DOI:10.1016/j.matchemphys.2020.122867

Czarnecki, R., Dziurka, D., and Lecka, J. (2003). "The use of recycled boards as the substitute for particles in the centre layer of particleboards," *Electronic Journal of Polish Agricultural Universities* 6(2), 1.

Davis, E., and Mott, N. (1970). "Conduction in non-crystalline systems. V. Conductivity, optical absorption and photoconductivity in amorphous semiconductors," *Philos. Mag.* 22, 903-922.

Deifallah, M., McMillan, P. F., and Cora, F. (2008). "Electronic and structural properties of two-dimensional carbon nitride graphenes," *The Journal of Physical Chemistry C* 112(14), 5447-5453. DOI: 10.1021/jp711483t

Ehtesabi, H., and Massah, F. (2021). "Improvement of hydrophilicity and cell attachment of polycaprolactone scaffolds using green synthesized carbon dots," *Materials Today Sustainability* 13, article 100075. DOI: 10.1016/j.mtsust.2021.100075

Fajrina, N., and Tahir, M. (2019). "A critical review in strategies to improve photocatalytic water splitting towards hydrogen production," *International Journal of Hydrogen Energy* 44(2), 540-577. DOI: 10.1016/j.ijhydene.2018.10.200

Fang, L. J., Li, Y. H., Liu, P. F., Wang, D. P., Zeng, H. D., Wang, X. L., and Yang, H. G. (2017). "Facile fabrication of large-aspect-ratio g-C_3N_4 nanosheets for enhanced photocatalytic hydrogen evolution," *ACS Sustainable Chemistry & Engineering* 5(3), 2039-2043. DOI: 10.1021/acssuschemeng.6b02721

Farjana, S. H., Tokede, O., and Ashraf, M. (2023). "Environmental impact assessment of waste wood-to-energy recovery in Australia," *Energies* 16(10), article 4182. DOI: 10.3390/en16104182

Girods, P., Dufour, A., Rogaurne, Y., Rogaurne, C., and Zoulalian, A. (2008). "Pyrolysis of wood waste containing urea-formaldehyde and melamine-formaldehyde resins," *Journal of Analytical and Applied Pyrolysis* 81(1), 113-120. DOI: 10.1016/j.jaap.2007.09.007

Grimm, D. (2008). "A combined experimental and theoretical approach towards the understanding of transport in one-dimensional molecular nanostructures," Tech. Univ. Chemnitz.

Han, H., Lou, Z. C., Wang, P., Wang, Q. Y., Li, R., Zhang, Y., and Li, Y. J. (2020).

"Synthesis of ultralight and porous magnetic g-C_3N_4/g-carbon foams with excellent electromagnetic wave (EMW) absorption performance and their application as a reinforcing agent for 3D printing EMW absorbers," *Industrial & Engineering Chemistry Research* 59(16), 7633-7645. DOI: 10.1021/acs.iecr.0c00665

Henriques, A., Paiva, N., Bastos, M., Martins, J., Carvalho, L., and Magalhaes, F. D. (2017). "Improvement of storage stability and physicochemical properties by addition of benzoguanamine in melamine-formaldehyde resin synthesis," *Journal of Applied Polymer Science* 134(32), article 45185. DOI: 10.1002/app.45185

Heyd, J., Scuseria, G. E., and Ernzerhof, M. (2006). "Hybrid functionals based on a screened Coulomb potential," *Journal of Chemical Physics* 124(21), article 219906. DOI: 10.1063/1.2204597

Jafari, T., Moharreri, E., Amin, A. S., Miao, R., Song, W. Q., and Suib, S. L. (2016). "Photocatalytic water splitting the untamed dream: A review of recent advances," *Molecules* 21(7), article 900. DOI: 10.3390/molecules21070900

Jia, C., Akbarpour, M. R., Gharamaleki, M. A., Ebadzadeh, T., and Kim, H. S. (2023). "Synthesis and characterization of novel NiTi-Ni_3Ti/SiC nanocomposites prepared by mechanical alloying and microwave-assisted sintering process," *Ceramics International* 49(14), 23358-23366. DOI: 10.1016/j.ceramint.2023.04.168

Kim, M. H., and Song, H. B. (2014). "Analysis of the global warming potential for wood waste recycling systems," *Journal of Cleaner Production* 69, 199-207. DOI: 10.1016/j.jclepro.2014.01.039

Kroke, E., Schwarz, M., Horath-Bordon, E., Kroll, P., Noll, B., and Norman, A. D. (2002). "Tri-s-triazine derivatives. Part I. From trichloro-tri-s-triazine to graphitic C_3N_4 structures," *New Journal of Chemistry* 26(5), 508-512. DOI: 10.1039/b111062b

Li, G., Huang, J. M., Wang, N. N., Huang, J. L., Zheng, Y. M., Zhan, G. W., and Li, Q. B. (2021). "Carbon quantum dots functionalized g-C_3N_4 nanosheets as enhanced visible-light photocatalysts for water splitting," *Diamond and Related Materials* 116, article 108242. DOI: 10.1016/j.diamond.2021.108242

Li, H., Guo, J. Q., Liu, A. K., Shen, X. C., Li, J. L., Liao, C. R., He, J., Liu, L. W., Wang, Y. P., Qu, J. L., Song, J., and Yan, W. (2023). "Long-wavelength excitation of carbon dots with dual-organelle targeting capability for live-cell imaging via STED nanoscopy," *Dyes and Pigments* 216, article 111383. DOI: 10.1016/j.dyepig.2023.111383

Li, S., Zhao, X., Zhang, Y., Chen, H., and Liu, Y. (2020). "Fluorescent N-doped carbon dots from bacterial cellulose for highly sensitive bacterial detection," *BioResources* 15(1), 78-88. DOI: 10.15376/biores.15.1.78-88

Li, T. H., Li, H. T., Pan, J. H., Guo, J. H., and Hu, F. R. (2015). "External-strain-induced Raman scattering modification in g-C_3N_4 structures," *Chinese Physics Letters* 32(10), 106201. DOI: 10.1088/0256-307X/32/10/106201

Li, X., Shen, R., Ma, S., Chen, X., and Xie, J. (2018). "Graphene-based heterojunction photocatalysts," *Applied Surface Science* 430, 53-107. DOI: 10.1016/j.apsusc.2017.08.194

Liu, H., Liu, M. L., Hou, P., and Huang, C. Z. (2017). "Preparation of element-doped fluorescent carbon dots and their applications in biological imaging," *Chinese Journal of Analytical Chemistry* 45(12), 1845-1856. DOI: 10.11895/j.issn.0253-3820.171296

Liu, M., Wang, Y., Wu, Y., and Wan, H. (2018). "Hydrolysis and recycling of urea formaldehyde resin residues," *Journal of Hazardous Materials* 355, 96-103. DOI:

10.1016/j.jhazmat.2018.05.019

Liu, X. J., Guo, M. L., Huang, J., and Yin, X. Y. (2013). "Improved fluorescence of carbon dots prepared from bagasse under alkaline hydrothermal conditions," *BioResources* 8(2), 2537-2546.

Lukowsky, D. (2002). "Influence of the formaldehyde content of waterbased melamine formaldehyde resins on physical properties of scots pine impregnated therewith," *European Journal of Wood and Wood Products* 60(5), 349-355. DOI: 10.1007/s00107-002-0324-y

Luo, W., Gan, J., Huang, Z., Chen, W., Qian, G., Zhou, X., and Duan, X. (2019). "Boosting HER performance of Pt-based catalysts immobilized on functionalized vulcan carbon by atomic layer deposition," *Frontiers in Materials* 6, article 251. DOI: 10.3389/fmats.2019.00251

Ma, L., Xiang, W. D., Gao, H. H., Wang, J. Y., Ni, Y. Y., and Lang, X. J. (2016). "Facile synthesis of tunable fluorescent carbon dots and their third-order nonlinear optical properties," *Dyes and Pigments* 128, 1-7. DOI: 10.1016/j.dyepig.2016.01.005

Majdoub, M., Anfar, Z., and Amedlous, A. (2020). "Emerging chemical functionalization of g-C_3N_4: Covalent/noncovalent modifications and applications," *ACS Nano* 14(10), 12390-12469. DOI: 10.1021/acsnano.0c06116

Mamba, G., and Mishra, A. K. (2016). "Graphitic carbon nitride (g-C_3N_4) nanocomposites: A new and exciting generation of visible light driven photocatalysts for environmental pollution remediation," *Applied Catalysis B-Environmental* 198, 347-377. DOI: 10.1016/j.apcatb.2016.05.052

Meier, R., Maple, J., Hwang, M. J., and Hagler, A. (1995). "Molecular modeling urea- and melamine-formaldehyde resins. 1. A force field for urea and melamine," *The Journal of Physical Chemistry* 99(15), 5445-5456. DOI: 10.1021/j100015a030

Norskov, J. K., Rossmeisl, J., Logadottir, A., Lindqvist, L., Kitchin, J. R., Bligaard, T., and Jonsson, H. (2004). "Origin of the overpotential for oxygen reduction at a fuel-cell cathode," *Journal of Physical Chemistry B* 108(46), 17886-17892. DOI: 10.1021/jp047349j

Ogita, N., Yamamoto, K., Hayashi, C., Matsushima, T., Orimo, S., Ichikawa, T., Fujii, H., and Udagawa, M. (2004). "Raman scattering and infrared absorption investigation of hydrogen configuration state in mechanically milled graphite under H_2 gas atmosphere," *Journal of the Physical Society of Japan* 73(3), 553-555. DOI: 10.1143/JPSJ.73.553

Perdew, J. P., Burke, K., and Ernzerhof, M. (1996a). "Generalized gradient approximation made simple," *Physical Review Letters* 77(18), article 3865. DOI: 10.1103/PhysRevLett.77.3865

Perdew, J. P., Ernzerhof, M., and Burke, K. (1996b). "Rationale for mixing exact exchange with density functional approximations," *The Journal of Chemical Physics* 105(22), 9982-9985. DOI: 10.1063/1.472933

Saraswat, V., and Yadav, M. (2020). "Carbon dots as green corrosion inhibitor for mild steel in HCl solution," *ChemistrySelect* 5(25), 7347-7357. DOI: 10.1002/slct.202000625

Sbacchi, M., Mamone, M., Morbiato, L., Gobbo, P., Filippini, G., and Prato, M. (2023). "Shining light on carbon dots: New opportunities in photocatalysis," *Chemcatchem* 15(16), 8. DOI: 10.1002/cctc.202300667

Segall, M. D., Lindan, P. J. D., Probert, M. J., Pickard, C. J., Hasnip, P. J., Clark, S. J., and Payne, M. C. (2002). "First-principles simulation: Ideas, illustrations and the

CASTEP code," *Journal of Physics-Condensed Matter* 14(11), 2717-2744. DOI: 10.1088/0953-8984/14/11/301

Selmi, W., Hosni, N., Naceur, J. B., Maghraoui-Meherzi, H., and Chtourou, R. (2023). "Effect of acids on optical and dielectric properties of g-C_3N_4 and the DFT simulation," *Optical and Quantum Electronics* 55(6), 517.

Shibayama, M., Shudo, Y., and Izumi, A. (2019). "Phenolic resins-recent progress of structure and properties investigations," *Macromolecular Symposia*. Wiley Online Library. pp. 1800156. DOI: 10.1002/masy.201800156

Singh, P., Kumar, S., and Kumar, K. (2023). "Biogenic synthesis of Allium cepa derived magnetic carbon dots for enhanced photocatalytic degradation of methylene blue and rhodamine B dyes," *Biomass Conversion and Biorefinery*. Early access, 1-19. DOI: 10.1007/s13399-023-05047-2

Souza, D. R., Caminhas, L. D., de Mesquita, J. P., and Pereira, F. V. (2018). "Luminescent carbon dots obtained from cellulose," *Materials Chemistry and Physics* 203, 148-155. DOI: 10.1016/j.matchemphys.2017.10.001

Tkatchenko, A., and Scheffler, M. (2009). "Accurate molecular van der Waals interactions from ground-state electron density and free-atom reference data," *Physical Review Letters* 102(7), article 073005. DOI: 10.1103/PhysRevLett.102.073005

Wang, D., Wang, W., Wang, Q., Guo, Z., and Yuan, W. (2017). "Spatial separation of Pt and IrO_2 cocatalysts on SiC surface for enhanced photocatalysis," *Materials Letters* 201, 114-117. DOI: 10.1016/j.matlet.2017.04.140

Wang, Y., Liu, X. Q., Liu, J., Han, B., Hu, X. Q., Yang, F., Xu, Z. W., Li, Y. C., Jia, S. R., Li, Z., and Zhao, Y. L. (2018). "Carbon quantum dot implanted graphite carbon nitride nanotubes: Excellent charge separation and enhanced photocatalytic hydrogen evolution," *Angewandte Chemie-International Edition* 57(20), 5765-5771. DOI: 10.1002/anie.201802014

Wareing, T. C., Gentile, P., and Phan, A. N. (2021). "Biomass-based carbon dots: Current development and future perspectives," *ACS Nano* 15(10), 15471-15501. DOI: 10.1021/acsnano.1c03886

Xia, C. L., Zhu, S. J., Feng, T. L., Yang, M. X., and Yang, B. (2019). "Evolution and synthesis of carbon dots: From carbon dots to carbonized polymer dots," *Advanced Science* 6(23), article 1901316. DOI: 10.1002/advs.201901316

Yang, C., Zhao, Z. Y., and Liu, Q. J. (2022a). "Regulating effect on photocatalytic water splitting performance of g-C_3N_4 via confinement of single atom Pt based on energy band engineering: A first principles investigation," *Applied Surface Science* 577, article 151916. DOI: 10.1016/j.apsusc.2021.151916

Yang, J., Guo, Z., and Yue, X. (2022b). "Preparation of carbon quantum dots from corn straw and their application in Cu^{2+} detection," *BioResources* 17(1), 604-615. DOI: 10.15376/biores.17.1.604-615

Zhang, C., Qin, D., Zhou, Y., Qin, F., Wang, H., Wang, W., Yang, Y., and Zeng, G. (2022). "Dual optimization approach to Mo single atom dispersed g-C_3N_4 photocatalyst: Morphology and defect evolution," *Applied Catalysis B-Environmental* 303, 120904. DOI: 10.1016/j.apcatb.2021.120904

Zhang, R., Zhang, X. M., Liu, S. W., Tong, J. W., Kong, F., Sun, N. K., Han, X. L., and Zhang, Y. L. (2021). "Enhanced photocatalytic activity and optical response mechanism of porous graphitic carbon nitride (g-C_3N_4) nanosheets," *Materials Research Bulletin* 140, article 111263. DOI: 10.1016/j.materresbull.2021.111263

Zhao, Z. W., Sun, Y. J., and Dong, F. (2015). "Graphitic carbon nitride based nanocomposites: A review," *Nanoscale* 7(1), 15-37. DOI: 10.1039/c4nr03008g

Zhong, R., Gu, J., Gao, Z. Z., Tu, D. Y., and Hu, C. S. (2017). "Impacts of urea-formaldehyde resin residue on recycling and reconstitution of wood-based panels," *International Journal of Adhesion and Adhesives* 78, 60-66. DOI: 10.1016/j.ijadhadh.2017.06.019

Zhu, K., Du, Y., Liu, J., Fan, X., Duan, Z., Song, G., Meng, A., Li, Z., and Li, Q. (2017). "Graphitic carbon nitride (g-C_3N_4) nanosheets/graphene composites: *In situ* synthesis and enhanced photocatalytic performance," *Journal of Nanoscience and Nanotechnology* 17(4), 2515-2519. DOI: 10.1166/jnn.2017.13439

Zhu, S. J., Song, Y. B., Zhao, X. H., Shao, J. R., Zhang, J. H., and Yang, B. (2015). "The photoluminescence mechanism in carbon dots (graphene quantum dots, carbon nanodots, and polymer dots): Current state and future perspective," *Nano Research* 8(2), 355-381. DOI: 10.1007/s12274-014-0644-3

Zinin, P. V., Ming, L. C., Sharma, S. K., Khabashesku, V. N., Liu, X. R., Hong, S. M., Endo, S., and Acosta, T. (2009). "Ultraviolet and near-infrared Raman spectroscopy of graphitic C_3N_4 phase," *Chemical Physics Letters* 472(1-3), 69-73. DOI: 10.1016/j.cplett.2009.02.068

Article submitted: January 16, 2024; Peer review completed: February 3, 2024; Revised version received and accepted: February 20, 2024; Published: February 27, 2024.
DOI: 10.15376/biores.19.2.2417-2435